Synthesis of Cu2ZnSnS4 (CZTS) Ink by an Easy Hydrothermal Method

Mahnaz Karbassi
Islamic Azad University Science and Research Branch
Saeid Baghshahi
Imam Khomeini International University
Nastaran Riahi-Noori
Niroo Research Institute
Roozbeh Siavash Moakhar (roozbehsiavash@gmail.com)
McGill University

Research Article

Keywords: CZTS, hydrothermal, doctor blade, thin film, solar cell

Posted Date: March 17th, 2021

DOI: https://doi.org/10.21203/rs.3.rs-294208/v1

Synthesis of Cu_2ZnSnS_4 (CZTS) Ink by an Easy Hydrothermal Method

Mahnaz Karbassi,[a] Saeid Baghshahi,[b,*] Nastaran Riahi-Noori,[c] Roozbeh Siavash Moakhar[c,*]

[a] Department of Materials Engineering, Science and Research Branch, Islamic Azad University, Simon Bulivar Blvd, 1477893855 ,Tehran, Iran
[b] Department of Materials Science and Engineering, Faculty of Engineering, Imam Khomeini International University, Persian Gulf Ave, 34149 16818, Qazvin, Iran
[c] Non-Metallic Materials Research Group, Niroo Research Institute (NRI), 1468613113, Tehran, Iran
*Corresponding authors, emails: baghshahi@ikiu.ac.ir, roozbehsiavash@gmail.com

Abstract.

The quadrilateral p-type semiconductor Cu_2ZnSnS_4 (CZTS) with a direct bandgap of 1.4 to 1.5 eV and a high absorption coefficient in the visible light range, is considered an excellent absorbent layer in the production of solar cells. The application of Cu_2ZnSnS_4 film absorbent materials is promising in the field of low-cost solar cell production. In this paper, a simple, efficient, controllable, and inexpensive solvothermal method is used to make the CZTS nanoparticles from zinc acetate, copper acetate, tin chloride, thiourea, and hexadecyl amine solvent. The ink was prepared from the CZTS powder and applied by the doctor Blade technique on soda-lime glass. The X-ray diffraction (XRD) and Raman spectroscopy analysis showed that the CZTS synthesis nanoparticles had a pure Kesterite structure. The thermo-gravimetric analysis showed about 12% of the loss weight of CZTS nanoparticles using field emission scanning electron microscopy, energy dispersive spectroscopy, dynamic light scattering, and zeta potential indicated that the synthesized nanoparticles had a strong absorption in the range of 125-477 nm with an average particle size of 300 nm and plate shape. The energy bandgap of CZTS nanoparticles was measured to be 1.49 eV using UV-Vis spectroscopy.

Keywords: CZTS; hydrothermal; doctor blade; thin film; solar cell

Introduction

In the last decade, copper-based quaternary semiconductor material Cu_2ZnSnS_4 (CZTS) was widely considered as a most promising absorber layer candidate for low-cost thin-film solar cells, owing to its high absorption coefficient ($>10^4$ cm^{-1}) and optimal bandgap (1.0–1.5 eV) which are ideal properties for the application under solar irradiation.[1-4] .The compounds such as copper-zinc, tin-sulfur accompanied by non-toxic and friendly environmental solvents have many photovoltaic technology applications.[5,6] The features of these compounds make them suitable for widespread and low-cost applications in the thin-film solar cells.[7] Furthermore, all the constituent elements of CZTS are naturally abundant and cheap, whereas the rare and expensive elements of In and Ga are employed in the well-known material of $CuIn_xGa_{1-x}$ $(S,Se)_2$ (CIGS / CIGSe).[5–8] Furthermore, all CZTS constituents are intrinsically abundant and inexpensive. In contrast, the CIGS constituents (In and Ga) are rare and expensive, making it an ideal candidate for producing cost-effective solar cells on a large scale.[4,5] Another benefit of CZTS compare to the other types of chalcopyrite-based solar cells is its suitability to fabricate high-performance solar cells using non-volatile methods.[6,7] One of the crucial issues in fabricating high absorbance coefficient thin-films finds the suitable ink and preparation methods due to non-toxic solvents and elements. Nowadays, most materials and solvents used in solar cells are not suitable from this point of view.[8,9] The function of a solar cell is highly sensitive to optical and electrical properties, which greatly depends on the crystalline structure and the absorbent material's composition. Therefore, to achieve the desired stoichiometry, understanding and optimizing the growth and formation of phases in photovoltaic materials is highly important. CZTS, as a quadruple combination, often involves dual and triple phases, which lead to difficult stoichiometry control. Therefore, it is necessary to have good control over the synthesis

parameters to obtain the desired phase materials.[10] Among different morphologies, nanocrystals (NCs) provide the bandgap engineering in which there are several electron-holes series per photon, and provide opportunities for using in high-performance photovoltaic devices. The NCs powders can be synthesized through a wet chemical route for preparing the nanoparticle inks.[11] Although the nonvacuum methods of manufacturing are attractive in terms of their low complex fabrication route, cost ,and scalability, the need for using toxic solvents and organic/metal solutions containing large amounts of pollutants to reduce the causes of cracks during the dissolution process is challenging.[12–15] Consequently, determining the desired properties of CZTS nanocrystals for inkjet printers requires designing new nanoparticle synthesis methods. The ability to control the crystallinity, morphology, and size of the CZTS nanocrystals provides an opportunity to examine further these properties' effects on the formation and synthesis behaviors. Among various process methods that lead to the formation of developed oxide nanoparticles, numerous strategies were implemented including using pre-made nano-reactors derived from surfactants,[16] ligands,[17] completed control reactions,[18] or poly-oxygen reactions including unique or oligomeric precursors which are specifically designed.[19] During the formation process, nanocrystals usually are created through reactions under atmospheric pressure and at a specific temperature. Previous nanoparticles from the sediment of chalcogenide Cu_2S_2 as the source of sulfide which directly interacts with Cu_xC and In_3C cations, showed that reaction paths usually lead to micron particles wheat-like structure.[7] Recent advances in the synthesis of colloidal semiconductor nanocrystals were promised using different techniques for preparing NCs.[20-22] The hydro/solvothermal process is an attractive method for large-scale synthesis of NCs powders among various techniques.[23] Hydrothermal reactions were widely used to synthesize NCs materials including TiO_2, ZnO, CdS, ZnS, and ZnSe.[24-28] Hydro/solvothermal

process was also used to synthesize CZTS.[29] Further, Colette et al.[30] used a solvothermal method in which hexadecyl amine (HDA) was used as a solvent to synthesize CZTS. According to the advantages of the hydrorthermal method (easy and using the aqueous solution), CZTS NCs were hydrothermally synthesized to use in absorber layers of solar cells. Then, CZTS films were formed via the doctor blade method. For the first time, we prepared CZTS NCs by autoclave during a short time (just 4 hr) in the present work. Besides, focused on the influence of relatively low temperatures between 300°C and 550°C, synthesis in high reactivity of zinc and tin was studied on the structural, compositional, morphological, and optical properties of quaternary kesterite CZTS NPs. The favorable results were obtained from the samples synthesized at relatively low temperature, which is comparable to the samples fabricated under expend.[31]

Experimental

The chemicals used in this study to synthesize the chemical composition of Cu_2ZnSnS_4 included: Cu $(CH_3COO)_2$. H_2O (Aldrich, 98%, 0.02 mol/L, copper source), Zn $(CH_3COO)_2$ (Aldrich, 99%, 0.01mol/L, zinc source), $SnCl_2$ (Riedel-de Haën, 98%, 0.01mol/L, tin sources), $SC(NH_2)_2$ (Thiourea, Fluka, 99%, TU, 0.1mol/L, sulfur sources), Thiourea was used without any further modifications. At first, the precursors were dissolved in 30 ml of ethanol. Then, hexadecyl amine ($C_{16}H_{35}N$, HDA) (previously dissolved in 50 ml of ethanol) was added to the mixture. Then, the mixture was continuously stirred for 5 hours. The resulting homogeneous, transparent solution was placed in an ultrasonic bath and finally in an autoclave container (internal Teflon liner). In a way, 50% of the container (50 ml) was filled). The autoclave was sealed for 4 hours at 200°C. Then, it was slowly cooled in room temperature. The resulting precipitate was filtered and washed several times with distilled water and pure ethanol to remove organic matter and dry in

the air. To produce the ink, the final obtained powder was added to alpha-terpineol (Aldrich, 96%), and the doctor blade technique applied the ink on a 20 ×10 mm^2 soda-lime glass. The film was dried on a hot plate at 150°C. The flow chart of process is shown in Fig. **1**.

The CZTS ink with a coating thickness of 2 µm was applied to the substrate surface in two steps. The films were heated at 300, 350, 400, 450, 500, and 550 °C for 20 minutes in a tubular furnace (laboratory tunnel furnace with quartz chamber) using reduced conditions of 95% N_2. The heat treatment was performed in the presence of pure sulfur and tin to prevent the presence of vapors and increase the grain size. The CZTS film formation process mechanism (reaction and growth) can be divided into three stages (equation (1)):

$$Cu^{2+}+Zn^{2+}+Sn^{4+}+Tu(\text{thiourea}) \longrightarrow \underbrace{[Cu(Tu)_n(H_2O)_X]^{2+}+ [Zn(Tu)_n(H_2O)_x]^{2+}+ [Sn(Tu)_n(H_2O)X]^{4+}}_{\text{Metal - Thiourea}} \quad (1)$$

After stirring and mixing the above mixture in ethanol, the color was initially blue to green-blue.

Then, it turned into a white transparent solution. In the next step, oxalic acid leads to dioxide formation (equation (2)):

$$[Cu(Tu)_n(H_2O)_X]^{2+} \rightarrow [Cu(Tu)_n(H_2O)_X]^{+} \quad (2)$$

In the final step, Tu and water trace (hydrated metal salt) are produced. Then, HS is decomposed into S_2 and H^+ ions (equation (3)).

$$[Cu(Tu)_n(H_2O)_X]^{2+}+[Zn(Tu)_n(H_2O)_x]^{2+} +[Sn(Tu)_n(H_2O)X]^{4+}+ S^2 \longrightarrow Cu_2ZnSnS_4 \quad (3)$$

The free ions of Cu^{2+} and Sn^{4+} are preferable to Zn^{2+} ions to join Tu in the final solution. After the whole Cu^{2+} ions reacted with Tu, then Zn^{2+} ions react with Tu.[4]

Thermal analysis (TGA) of CZTS samples performed under N_2 gas environment up to 600°C. Fig. **2** showed that the first weight loss of CZTS occurred at a relatively low temperature (240°C) with a significant amount of volatile substances (about 12% of the weight). This weight loss corresponds to thiourea decomposition.[6] It is worth noting that the complete elimination of volatile substances with a higher weight loss occurs at 600°C in the same samples.

DLS technique was used to determine the distribution of small particles in the slurry or polymers in the solution. The small particles in the slurry are constantly transported in a certain speed due to Brownian motion. Brownian motion is particles' movement due to random collisions with atoms or molecules of gas or liquid that surround the particles. An important feature of Brownian motion is that small particles move quickly, but large particles move slowly. If small particles are illuminated by a light source such as a laser, the light is scattered in all directions. Due to the moving particles, the constructive and destructive phase of dispersion light causes the oscillation in intensity.

The film's crystal structure was determined by an X-ray Diffraction (XRD, D8-Advance Bruker) applied the 2θ range 20° to 80° with $Cu_{K\alpha}$ radiation (λ= 0.15406 nm), scanning speed of 10°/min, and gazing angle of 0.1°. The crystallite size of CZTS was determined using the full width at half maximum of diffraction peaks (L) using Scherer's equation (equation (4)):

$$\beta = \frac{k\,\lambda}{L\cos\theta} \tag{4}$$

Where β is the line broadening at half of the maximum intensity, and λ is the X-ray wavelength (for λ =1.5418 cm^{-1}, k=0.9). Raman spectrum was performed using a Jobin-Yvon HR800 Raman microscope with an excitation wavelength of 488 nm. The bonding property of as-synthesized NPs examines by the FTIR method in the wavelength range of 500–4000 nm (Perkin Elmer

1760-X). The film's morphology and chemical composition were investigated by field emission scanning electron microscopy (FESEM, HITACHI S-4160) equipped with an energy dispersive spectroscopy (EDS). The thermal properties of CZTS film were studied using the thermogravimetric analysis (TGA) (TA Instruments TGA 2950 system). The optical properties of CZTS films were investigated employing a UV–Visible spectrophotometer between 400–1100 nm wavelengths (Shimadzu, UV-3600), by which the bandgap of CZTS films was also calculated.

Dynamic light scattering (DLS) was used to determine the average size of particles and size distribution in dilute suspensions. Cuvettes from VWR with Nanosizer ZS from Malvern Instruments (Herrenberg, Germany). Detection was done using non-invasive back-scattering in detector channels with the angles of 173 and 256 degrees. A 4.0 MW He-Ne laser light source with a 633 nm emission rate was employed. The average of particles' hydrodynamic diameter o was derived from the time evolution of scattered light intensity using the Stokes-Einstein equation. Before the measurement, the solution was centrifuged for 15 minutes using an ultrasonic bath (40, 35 kHz, 460/H Elma). All data were collected at room temperature (25°C).[32] The DLS of samples were measured based on time-dependent spatial oscillation fluctuations, and these data were used to calculate the emission factor and particle size. The relation between the particle size and its emission factor is defined in the Stokes-Einstein equation (5):

$$D = \frac{KT}{3\pi\,\eta D} \tag{5}$$

Where, D is the penetration coefficient, T is the absolute temperature, η is liquid viscosity, K is the Boltzmann constant, and d is the particle size. To obtain reliable information on particle size, the temperature should be kept constant about ± 0.1K. The Stokes-Einstein equation is valid only

for non-spherical, flat, rigid particles and is approximate for others. Zeta potential using Zeta PALS Zeta Potential Analyzer, Brookhaven Instruments Corporation, US) using a low and high electric field, E = 137 Vcm^{-1} and 274 Vcm^{-1}, using palladium electrodes and Zeta potential amounts measured from two fields which were tested at least 10 times and constant.

Results and Discussion

The crystallographic structure of CZTS films synthesized in different temperatures is shown in Fig. **3**. Similarly, in all specimens, peaks at 28.8, 33, and 47.3^o are present, which are related to the crystallographic planes (112), (200), and (220) of the tetragonal kesterite structure, respectively (JCPDS Card No. 26-0575). In sample D, two other peaks appeared at 47 and 56^o, which are related to CTS. In sample E, the intensity of peak at 47^o is relatively high. The secondary phase of CTS is one of the main sub-phases of CZTS. The peak of SnS (secondry phase) was determined in samples D and E at an angle of 43 degrees and in samples F at 25 and 30 degrees. Secondary phases have high Electrical conductivity and can create electron transfer paths in photovoltaic devices, so they are not suitable for a solar cell. In fact, Secondary phases function as traps for electrons and holes.[31]

The CTS and Sn_xS_y phases effectively reduce the moving electrons and increase the position holes and, thus, on the solar cell's efficiency. Peak intensities in samples E and F are sharper than the other ones which indicate improved crystallinity by increasing the synthesis temperature.

Further, the average crystallite particle size of samples calculated by Scherrer (Fig. **4**). According to the results, the increase in the synthesis temperature (300-550°C) significantly affected the composition and crystallinity. The grain size was between 125 and 477 nm (300°C: 125nm, 350°C: 152 nm, 400°C: 205nm, 450°C: 320nm, 500°C: 385nm, 550°C: 477 nm).

The X-ray diffraction analysis, it is possible to fully match the peaks of CZTS polymorphs and secondary phases (such as CTS and Sn_xS_y); therefore, the results of XRD analysis measurements are insufficient to describe the separation of kesterite and CTS phase. Raman spectroscopy is a common study method to investigate the structures of chalcogenide and kesterite. The Raman spectra of synthesized CZTS sample films are shown in Fig. **5**.

All films generally have a strong peak at 336 cm^{-1} and a fairly weak peak at 287 cm^{-1}. There is no definite peak in the samples synthesized at 300 and 350 degrees. Comparing the samples' shape indicates that the intensity of the peaks slowly increases with increasing temperature. Raman results indicate that the ink prepared by the solvothermal method had a pure kesterite phase which is compatible with XRD peaks. It is worth noting that there is a trace of secondary phases in two of the samples (A and B). In other samples, more peaks at 303 and 224 cm^{-1} are detected which is related to tetragonal CTS and Sn_xS_y phases, relatively.[33]

To better describe these volatile compounds' identity, FTIR analysis was performed at intervals of 500 to 4000 cm^{-1} and showed different peaks with the most intense peaks at 3330, 1629, and 1415 cm^{-1} (Fig. 5). The strong peak absorbed in 2938 and 2369 cm^{-1} is due to the S-H bond. The peaks at 1629 and 1415 cm^{-1} are due to the C = S and NH_2 bond, respectively. Moreover, the removal of organic compounds shown; the results were following the TGA curve.[34]

FESEM was used to analyze the surface morphology of CZTS samples. As can be observed from Fig. **7**, the CZTS films consist of agglomerated and porous form interconnected spherical grains. By increasing the temperature, CZTS particles grew plate shape which became isolated. The sample heated at 400°C consisted of the platelet particles with a thickness of 40-50 nm. While the sample heated at 500°C consisted of petal-like particles with a thickness of 30-40 nm. In the sample heated at 550°C, the particles turned into a curved petal. It can be seen that the length of

particles has increased from 125 to 477 nm by increasing temperature which showed in Fig. **7**. The CZTS fine grains were connected to form the dangling bonds and chain-similar matrix. Also, the results are matched with the XRD and Raman spectroscopy results discussed above. Due to the XRD, Raman Spectra, and FESEM analysis results, sample E, structurally, and morphologically showed better properties and studies.

The EDS analysis indicate the situation of (Cu-Zn-S-Sn), (Al-Ca-Si), and (Au) elements, which can be referred to as the CZTS layer, the substrate, and the coating, respectively. In sample E, the composition proportion of CZTS layer is Cu/Zn/Sn/S =2.8/1.5/0.95/5.5.

The quantities results show that the chemical composition of sample heated at 500ºC involved zinc - abundant and tin – needy (Fig. **8**). According to studies by Bandres[35] and Chen et al.,[36] the best result to use in a solar cell can be achieved in zinc-rich and the copper-poor conditions. Zinc is critical in the final performance of device.

The UV-Vis Transmittance spectrums of samples are drawn in Fig. **9**. The size range of CZTS particles indicated that the intense absorption about 280 nm. The bandgap of CZTS nanoparticles (direct bandgap) was determined from the transmittance spectrum using the Tauc equation (6):

$$\alpha h\vartheta = A(h\vartheta - Eg)^2 \quad (6)$$

where

α is the absorption coefficient (cm^{-1}),

h is the Plank's constant (J-s),

ν is the frequency of radiation (Hz),

A is an appropriate constant, and E_g is the bandgap (eV).

The sample bandgap is in the range of 1.49 to 1.62 eV. According to the graph (hν) versus $(\alpha h\nu)^2$ as shown in Fig. **9**, the bandgap energy in the synthesized sample at 500°C has the best value

(1.49 eV energy band). According to several studies, the bandgap of samples is in the range of 1.49 to 1.62 eV; for example, in Akhanda et al.[37], the bandgap energy of similar materials used in the present study is the bandgap energy of 1.46 to 1.53 eV. A sample with a lower bandgap length has a higher potential for solar applications. Therefore, among the samples synthesized in the autoclave and hydrothermal method, sample E synthesized at 500°C

Fig. **10** shows the particle size distribution measured by DLS (providing a hydrodynamic average diameter of 270 nm and a Polydispersity Index (PI) of 0.039 which indicates a monodisperse suspension) compared to that measured by FESEM images; giving a size distribution peaked about 300±30 nm. The zeta potential in the prepared ink is 24 millivolts which is provided by strong bonding.

Conclusions

To improve the performance of solar cell, an alternative CZTS film structure was proposed in this work. The benefits of using solvothermal technology and the doctor blade printings were demonstrated in this paper. Solvothermal made the ink with zinc copper, copper acetate, zinc acetate, tin chloride, and thiourea materials. The XRD analysis indicated the kesterite structure. Raman analysis results confirmed the formation of the pure phase of CZTS nanoparticles. The coating agent was displayed on the surface of CZTS nanoparticles prepared by the FT-IR spectrum. Based on TGA analysis results, the weight loss of CZTS occurred at a relatively low temperature, which corresponds to the decomposition of thiourea. The FESEM micrographs indicate that CZTS nanoparticles synthesized in 150 and 200ºC temperatures were agglomerated. FESEM images of CZTS thin films show the morphology first is dense and more uniform and compact after annealing. In the formation of CZTS thin layers, the temperatures played a vital

role in the final microstructure. The best sample was prepared at 500ºC. The considerable number of CZTS particles was calculated in the size of 350-650 nm range. The UV-Vis results indicated that the optical bandgap of CZTS nanoparticles is 1.49 eV. In general, we concluded that the solvothermal procedure is a very promising technique for the aim of thin-film solar cell production, which can certainly pave the way towards using cost-effective and industrial friendly method for large-scale fabrication of CZTS solar cells.

References

[1] Mostafa Boshta, Simona Binetti, Alessia Le Donne, Mohamed Gomaa and Maurizio Acciarri, "A chemical deposition process for low-cost CZTS solar cell on flexible substrates" , *Materials Technology: Advanced Performance Materials*, vol. 32, no. 4, pp. 251–255, 2017.

[2] A. G. Kannan, T. E. Manjulavalli, and M. Thambidurai, "Photo conversion efficiency of CZTS solar cells fabricated using ZnO as a buffer layer," *Int. J. ChemTech Res.*, vol. 10, no. 6, pp. 598–604, 2017.

[3] G. Grincienė, V.Pakstas, *et al.*, "Properties and characterization of CZTS nanoparticles prepared by microwave heating irradiation," *chemija*, vol. 29, no. 1, pp. 29-40, 2018.

[4] M. Karbassi, S. Baghshahi, N. Riahi-Noori, and R. S. Moakhar, "Deposition of Cu_2ZnSnS_4 films by doctor blade printing using a one-step microwave heated ink as an absorber layer for solar cells," *Ceram. Int.*, vol. 46, no. 2, pp. 2325–2331, 2020.

[5] H. Zheng, A. WEIa, and H. Xiong, "Influence Of Deposition Parameters On The Morphology, Structural And Optical Properties Of Cu_2znsns_4 Thin Films Grown By Solvothermal Method," *Chalcogenide Lett.*, vol. 15, no. 6, pp. 327–337, 2018.

[6] K. Abid Hubeatir, F.Kamil, A. A. Al-Amiery, A. A.H. Kadhum, Mohamad, A. B., "Polymer solar cells with enhanced power conversion efficiency using nanomaterials and laser techniques", *Materials Technology,* vol. 32, no.5, pp.279-298, 2017.

[7] W.Ch Oh, , K.Y. Cho, Ch.H Jung, Y.Areerob,"The viability of rumpled La_2CrFeW_6-CdSe perovskite wrapped by graphene for a viable efficiency and icreased utilization of dye-sensitized solar cells," Materials Technology, vol. 34, no. 5, pp. 247–257, 2019.

[8] A. Méndez-López, A. Morales-Acevedo, Y. J. Acosta-Silva, and M. Ortega-López, "Synthesis and characterization of colloidal CZTS nanocrystals by a hot-injection method," *J. Nanomater.*, vol. 2016, 2016.

[9] K. Pooput, "Synthesis and Characterization of Aqueous Cu_2ZnSnS_4 Nanoparticles for Antimicrobial Applications." Drexel University, 2014.

[10] R. Siavash Moakhar, S. Gholipour, S. Masudy-Panah, A. Seza, A. Mehdikhani, ,N. Riahi-Noori , S .Tafazoli, , N. Timas, Y. Lim, "Recent Advances in Plasmonic Perovskite Solar Cells," *Advanced Science*, vol. 7, n.13, pp. 1–19, 2020.

[11] M. Boshta, S. Binetti, A. Le Donne, M. Gomaa, and M. Acciarri, "A chemical deposition process for low-cost CZTS solar cell on flexible substrates", *Mater. Technol.*, vol. 32, no. 4, pp. 251–255, 2017.

[12] Z . Shadrokh, A. Yazdani and H. Eshghi, "Study on Structural and Optical Properties of Wurtzite Cu2ZnSnS4 Nanocrystals Synthesized via Solvothermal Method", *Int. J. Nanosci. Nanotechnol.*, vol.13, n. 4, pp. 359-366, 2017 .

[13] A. Méndez-López, A. Morales-Acevedo, Y. J. Acosta-Silva and M. Ortega-López, "Synthesis and characterization of colloidal CZTS nanocrystals by a hot-injection method" *, J. Nanomater.* **,** vol. 2016**,** pp.1-7, 2016.

[14] K. Pooput, "Synthesis and Characterization of Aqueous Cu_2ZnSnS_4 Nanoparticles, nor

Antimicrobial Applications", Drexel University: Philadelphia, United States, pp. 24, 2014.

[15] M. Z. Ansari, S. Munjal and N. Khare, "Intrinsic strain dependent redshift in optical band gap of Cu_2ZnSnS_4 nanostructured thin films", *Thin Solid Films*, vol.657**,** pp. 95-100, 2018.

[16] S. L. J. Engberg, "Cu_2ZnSnS_4 Nanoparticle Absorber Layers for Thin-Film Solar Cells" Technical University of Denmark: Lyngby, Denmark, pp. 33, 2016.

[17] G. Gogoi, S. Arora, N. Vinothkumar, De M and Qureshi M, "Quaternary semiconductor Cu $_2ZnSnS_4$ loaded with MoS 2 as a co-catalyst for enhanced photo-catalytic activity", *RSC Adv.*, vol. 5, n. 51 pp. 40475-40483, 2015.

[18] A. Ali, W. A. Syed, W. Arif, S. Ahmed and M. Ghufran "Environment friendly nanoparticles of quaternary compound $Cu_{0.5}Mg_xSnS_4$ for possible photovoltaic and photo-catalytic applications", *Mater. Res. Express*, vol. 6, n. 9, pp. 0950b5, 2019.

[19] N. A. Bakr, Z. T. Khodair and S. M. Hassan, "Effect of substrate temperature on structural and optical properties of Cu_2ZnSnS_4 (CZTS) films prepared by chemical spray pyrolysis method" *Res. J. Chem. Sci.* vol. 6, n. 9, 2231 606X, 2015.

[20] V. Buissette, M. Moreau, T. Gacoin, J. P. Boilot, J. Y. Chane-Ching and T. Le. Mercier, "Colloidal Synthesis of Luminescent Rhabdophane $LaPO_4$: $Ln_{3+.\ x}$ H_2O (Ln= Ce, Tb, Eu; x≈ 0.7) Nanocrystals", *Chem. Mater,* vol. 16**,** n. 19, pp. 3767-3773, 2004.

[21] R .Gonzalez-McQuire, J. Y. Chane-Ching, E .Vignaud, A. Lebugle and S. Mann, "Synthesis and characterization of amino acid-functionalized hydroxyapatite nanorods", *J. Mater. Chem.*, vol. 14, n. 14, pp. 2277-2281, 2004.

[22] S. E. Habas, H. A. S. Platt, M. F. A. M. Van Hest and D. S. Ginley, "Low-cost inorganic

solar cells: from ink to printed device", *Chem. Rev.* vol.110, n. 11, pp. 6571-6594-, 2010.

[23] A. Khare, A. W. Wills, L. M. Ammerman, D. J. Norris and E. S. Aydil, "Size control and quantum confinement in Cu2ZnSnS4 nanocrystals", *Chem. Commun.* vol.47, n. 42, pp.11721, 2011.

[24] C. Steinhagen, M. G. Panthani, V. Akhavan, B. Goodfellow, B. Koo and B. A. Korgel, "Synthesis of Cu_2ZnSnS_4 nanocrystals for use in low-cost photovoltaics", *J. Am. Chem. Soc.*, vol. 131, n. 35, pp**.** 12554-12555, 2009.

[25] Q. Guo, H. W. Hillhouse and R . Agrawal, "Synthesis of Cu_2ZnSnS_4 nanocrystal ink and its use for solar cells", *J. Am. Chem. Soc.*, vol. 131, n.33 , pp. 11672-11673, 2009.

[26] M. Rajamathi and R. Seshadri "Oxide and chalcogenide nanoparticles from hydrothermal/solvothermal reactions", *Curr. Opin. Solid State Mater. Sci.*, vol. 6**,** n. 4, pp.337-345, 2002.

[27] H. Zhang, X. Ma, Y. Ji, J. Xu and D. Yang, "Single crystalline CdS nanorods fabricated by a novel hydrothermal method", *Chem. Phys. Lett.*, vol. 377, n. 5, pp. 654-657, 2003.

[28] L. Wang, J. Dai, X . Liu, Z. Zhu, X. Huang and P. Wu "Morphology-controlling synthesis of ZnS through a hydrothermal/solvthermal method", *Ceram. Int, vol.* 38, n. 3 , pp. 1873-1878, 2012.

[29] H. Gong, H. Huang, M. Wang and K. Liu, "Characterization and growth mechanism of ZnSe microspheres prepared by hydrothermal synthesis", *Ceram. Int.* , vol. 33, n. 7, pp. 1381-1384, 2007.

[30] T. Wada, S. Nakamura, T. Maeda,"Ternary and multinary Cu-chalcogenide photovoltaic materials from $CuInSe_2$ to Cu_2ZnSnS_4 and other compounds", *Prog. Photovoltaics Res. Appl.* vol. 20, n. 5, pp. 520- 525 , 2012.

[31] W. Hongxia, “Progress in thin film solar cells based on Cu_2ZnSnS_4”, *Int. J. Pho-toenergy*, vol. 2011 ,pp.1-10, 2011.

[32] J. Chen, B. Yang, W. Fengchao, P. Xiaogai, “Fabrication of Cu_2ZnSnS_4 Thin Films Based on Facile Nanocrystals-Printing Approach with Rapid Thermal Annealing (RTA) Process”, *Coatings*, vol. 9, n. 2, pp. 1-11, 2019.

[33] K.C. Wanga, P. Chen, and C.M. Tseng, “Facile one-pot synthesis of Cu_2ZnSnS_4 quaternary nanoparticles with microwave-assisted method”, CrysteEngComm, vol. 15, n. 46 **,** pp. 9863-9870 , 2013.

[34] J. B. Li, V. Chawla, and B. M. Clemens, “Investigating the role of grain boundaries in CZTS and CZTSSe thin film solar cells with scanning probe microscopyc*, Adv. Mater.* **, vol. 24**, n. 6, pp. 720-723, 2012.

[35] R. D. Bandres,“Preparation and characterization of $Cu_{2-x}Zn_{1+\ y}SnS_4$ for thin films solar cells”, (University of Trento: Trento, Italy), P.2, 2016.

[36] J. Zhang and Y. G. Jung, “Advanced ceramic and metallic coating and thin film materials for energy and environmental applications”, Springer, vol. 22, 2018.

[37] A. H. Pinto, S. W. Shin, E. Isaac, T. R. Knutson, Aydil E S and R. L. Penn, “ Controlling Cu_2ZnSnS_4 (CZTS) phase in microwave solvothermal synthesis“, *J. Mater. Chem. A,* vol.5, n. 44, pp. 23179- 23189, 2017.

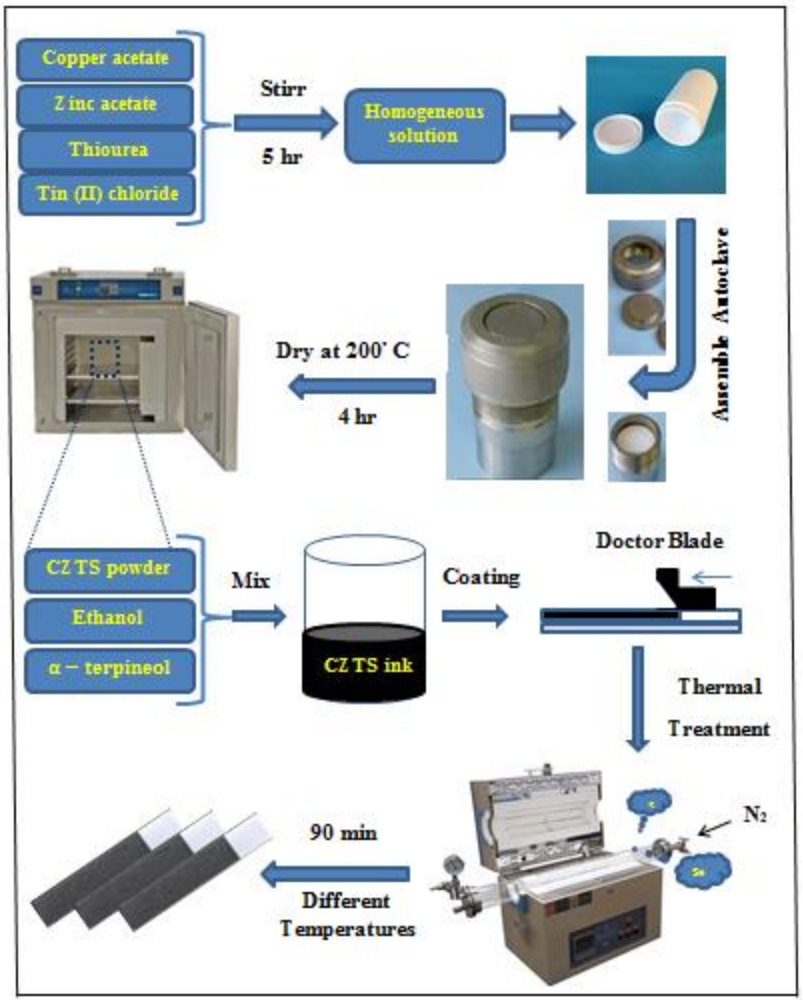

Fig. 1- Flow diagram of the CZTS ink and film synthesis.

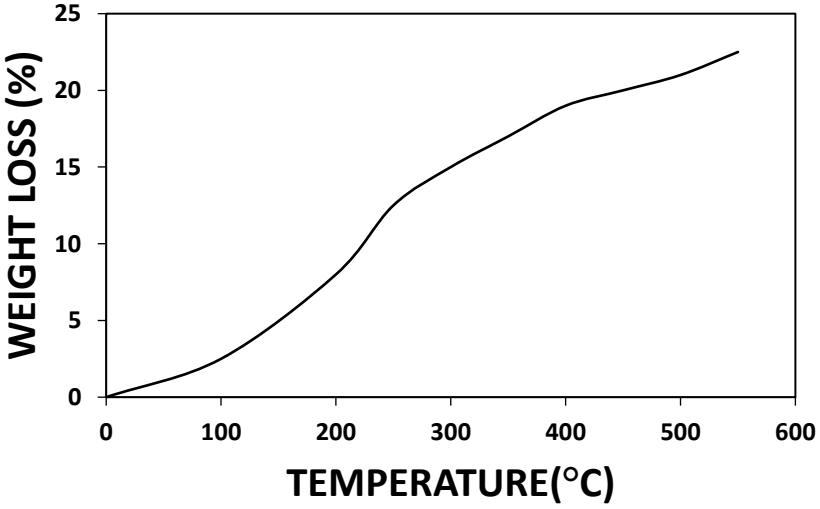

Fig. 2- TGA results of synthesized CZTS.

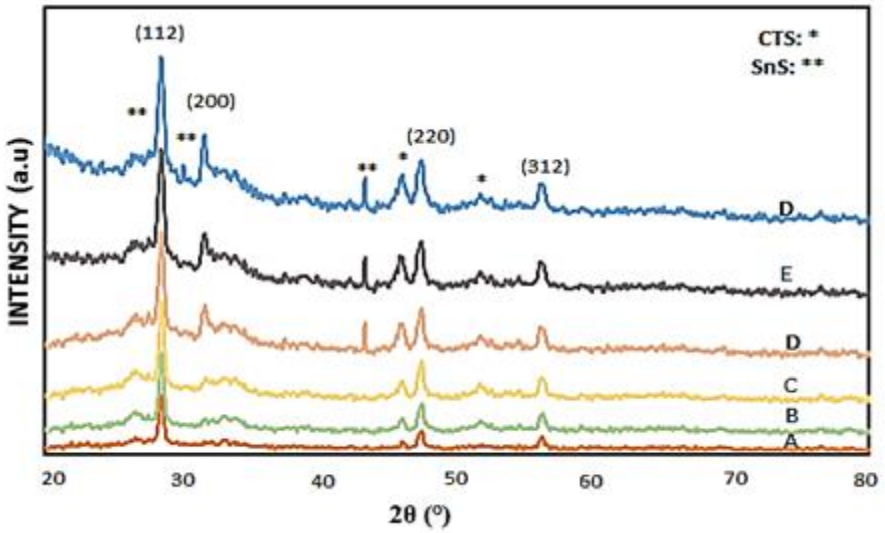

Fig. 3- XRD Pattern of the CZTS layer heated at A) 300, B) 350, C) 400, D) 450, E) 500, and F) 550°C.

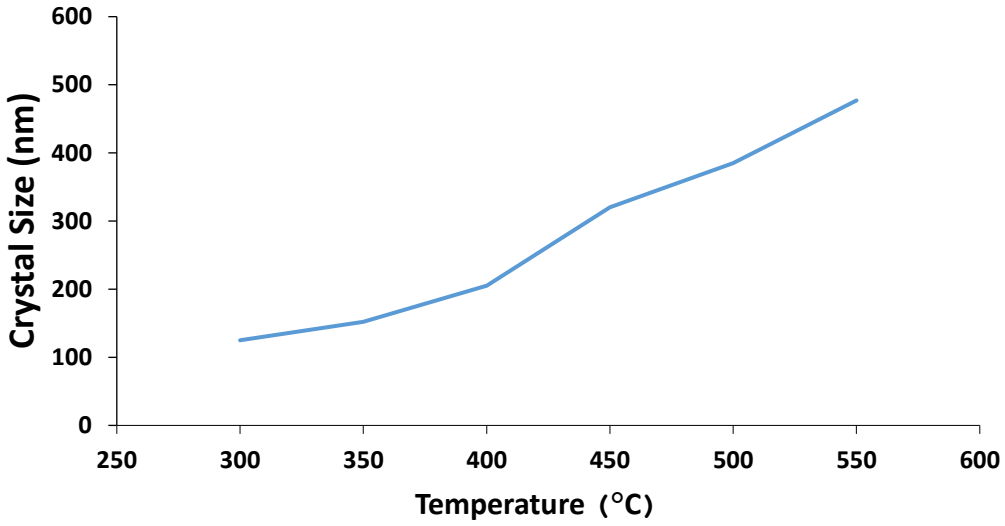

Fig. 4- The average crystallite size of the samples.

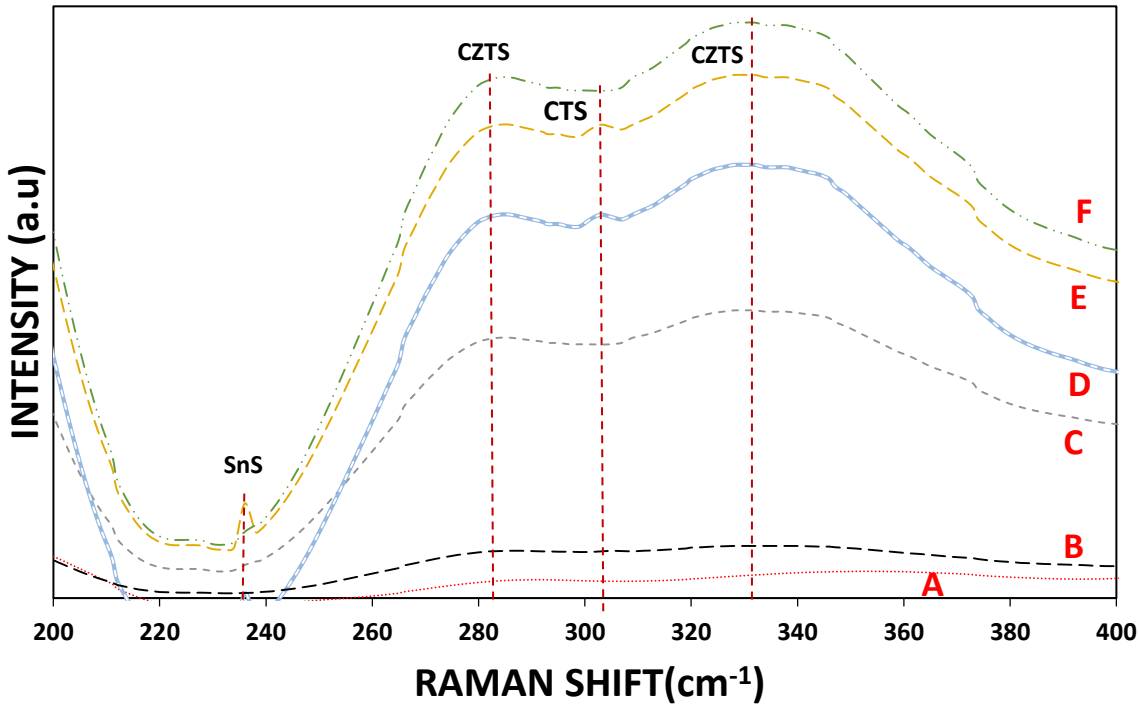

Fig. 5- Raman spectra of CZTS films heated at A) 300, B) 350, C) 400, D) 450, E) 500, and F) 550 °C.

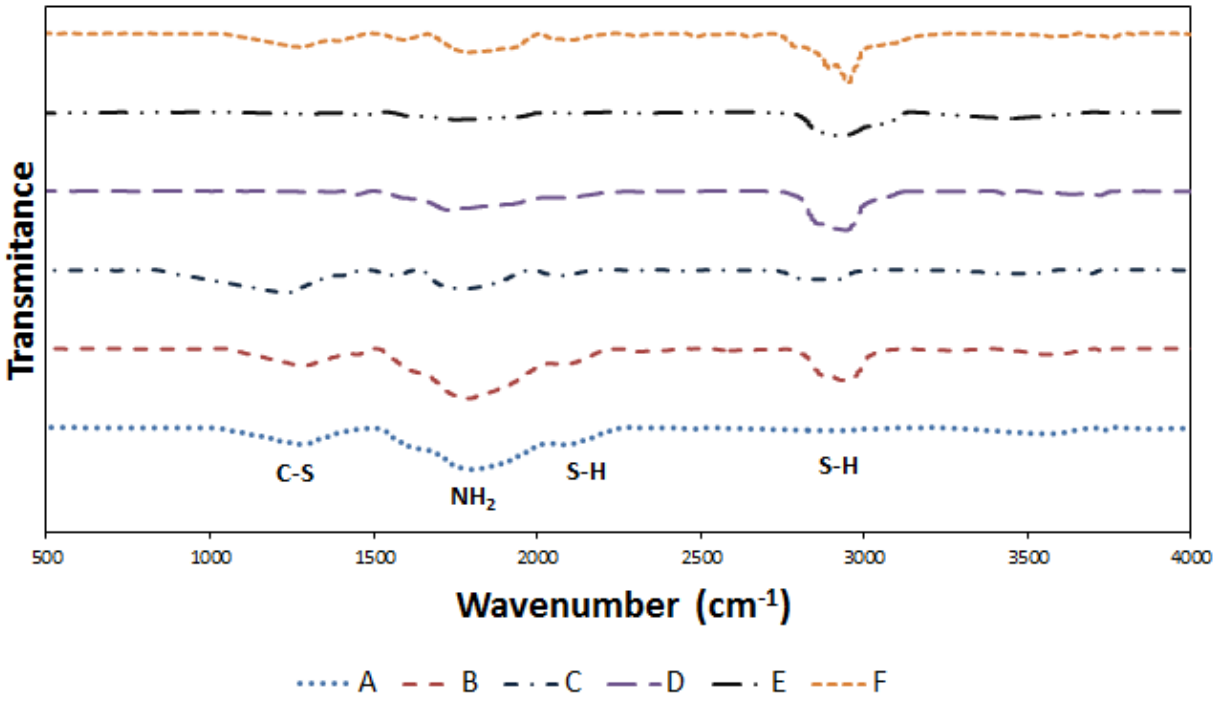

Fig. 6- FTIR spectra of the CZTS samples heated at A) 300, B) 350, C) 400, D) 450, E) 500, and F) 550°C.

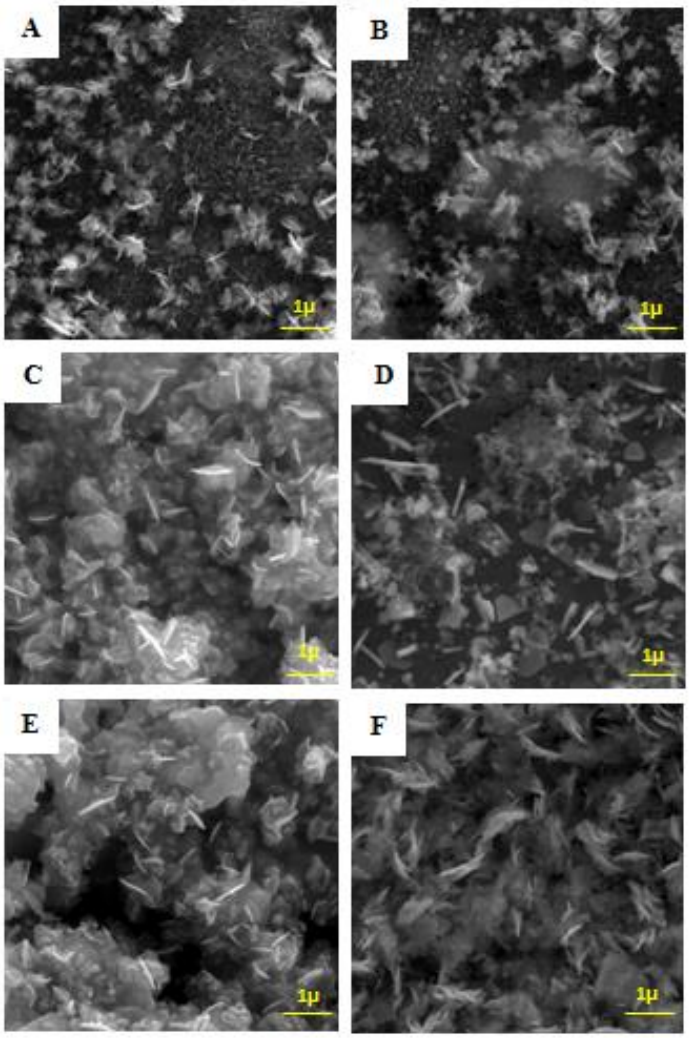

Fig. 7- FESEM of CZTS layer prepared at (A) 300, (B) 350, (C) 400, (D) 450, (E) 500 and (F) 550ºC.

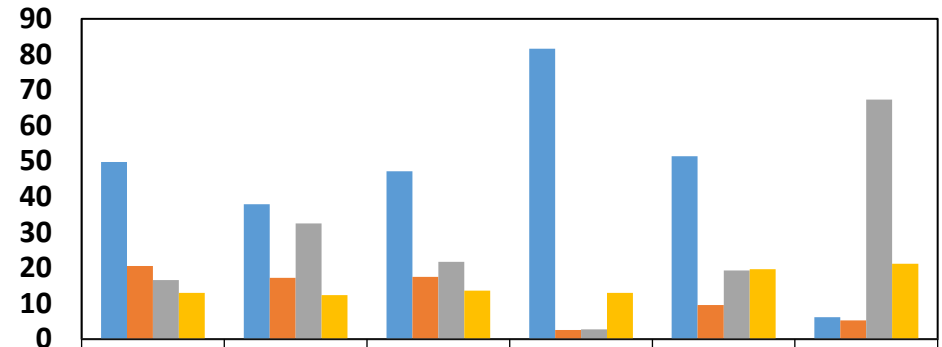

	A	B	C	D	E	F
Sn	49.8	37.9	47.2	81.6	51.4	6.2
Zn	20.6	17.2	17.5	2.6	9.6	5.3
Cu	16.6	32.5	21.7	2.8	19.3	67.3
S	13	12.4	13.6	13	19.7	21.2

Fig. 8- Comparison of the EDS analysis of the CZTS layer synthesized at A) 300, B) 350, C) 400, D) 450, E) 500 and F) 550ºC.

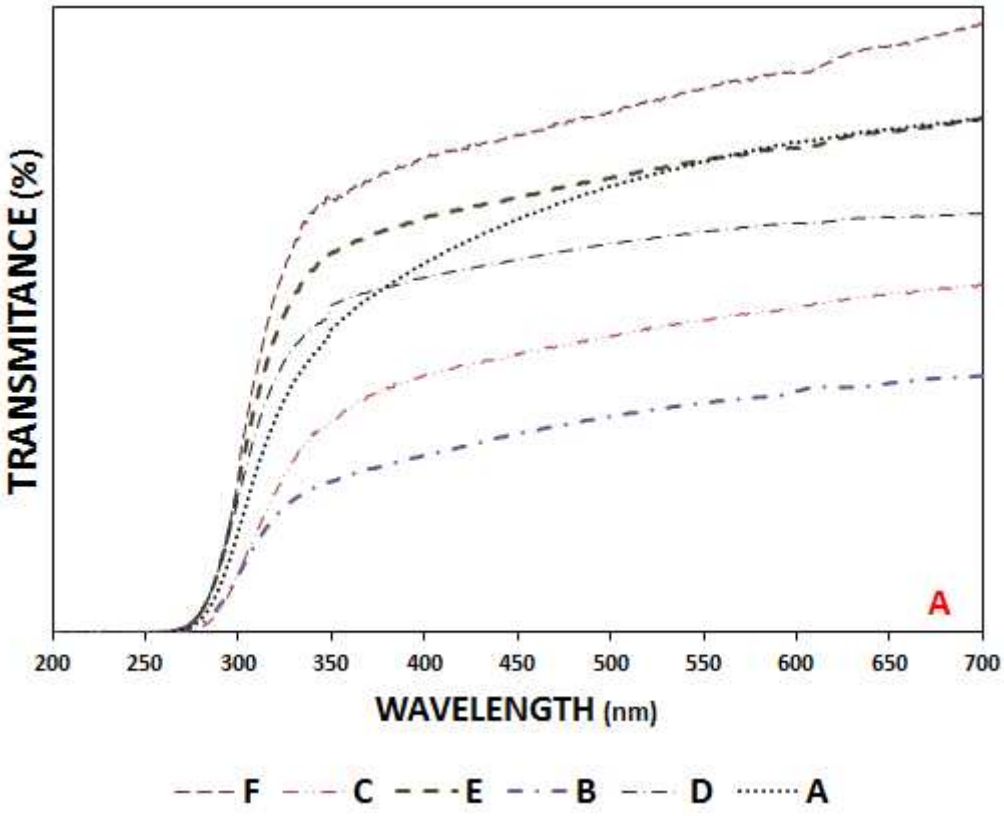

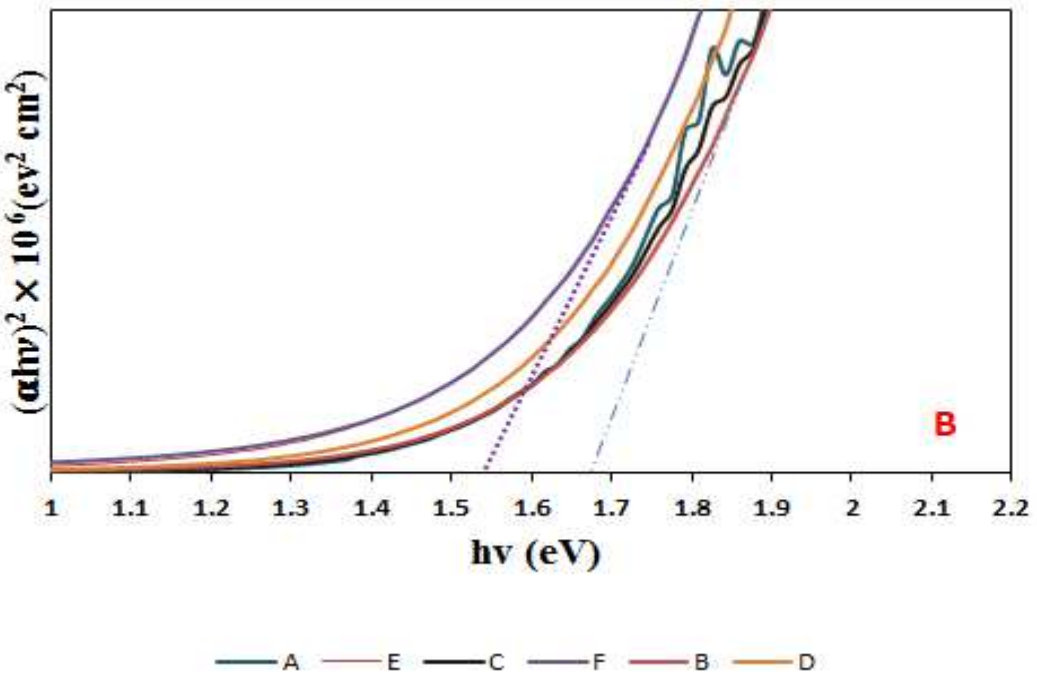

Fig. 9- A) Transmittance spectra of the samples heated, B) The Tauc plot of the samples heated at A) 300, B) 350, C) 400, D) 450, E) 500 and F) 550°C.

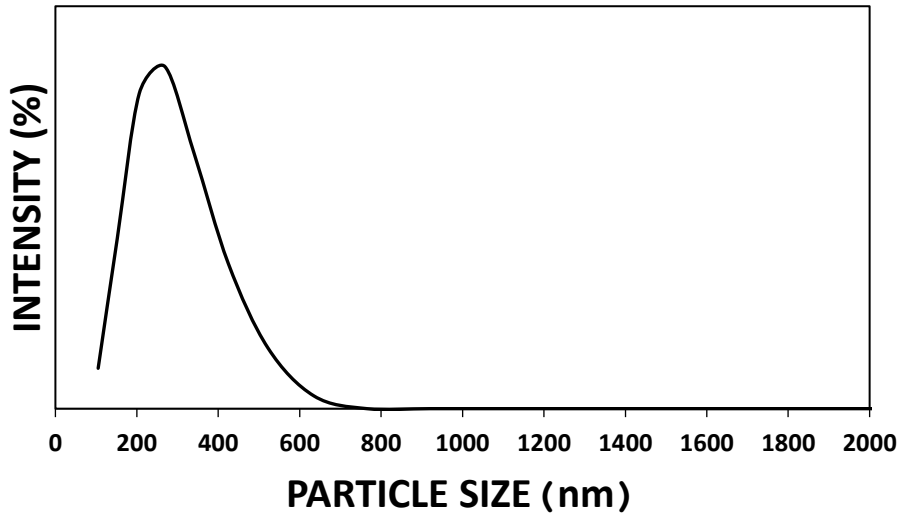

Fig. 10- The particle size distribution curve of the synthesized powder at 500°C.

Figures

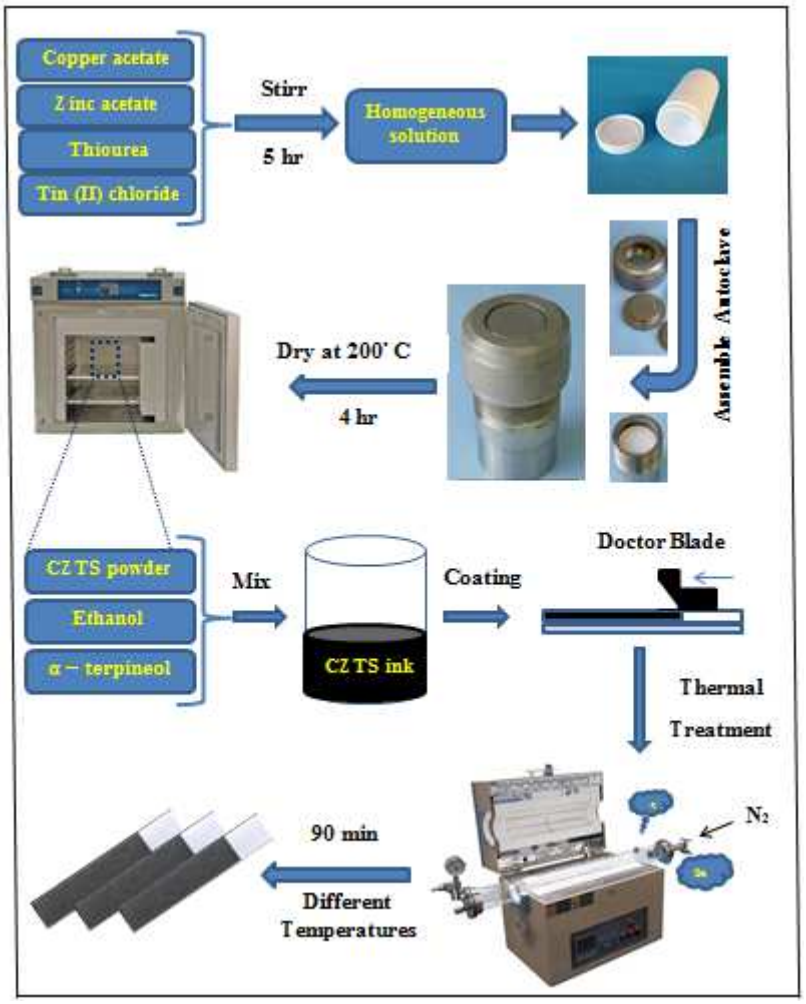

Figure 1

Flow diagram of the CZTS ink and film synthesis.

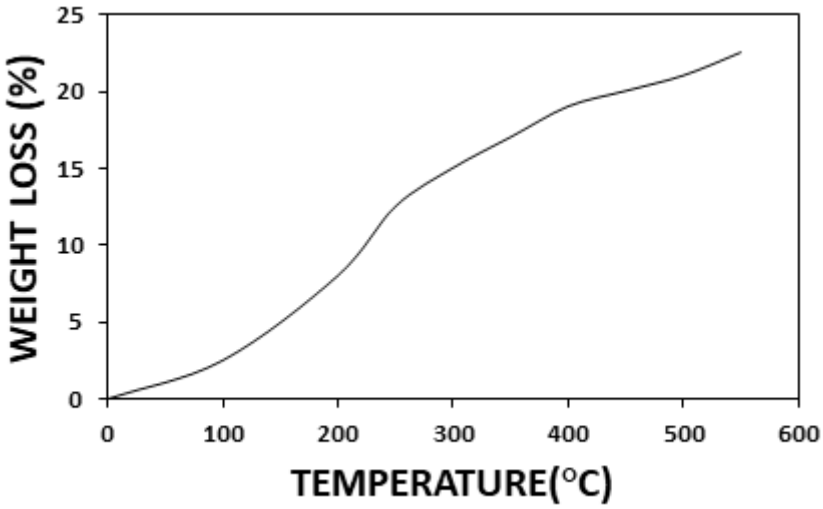

Figure 2

TGA results of synthesized CZTS.

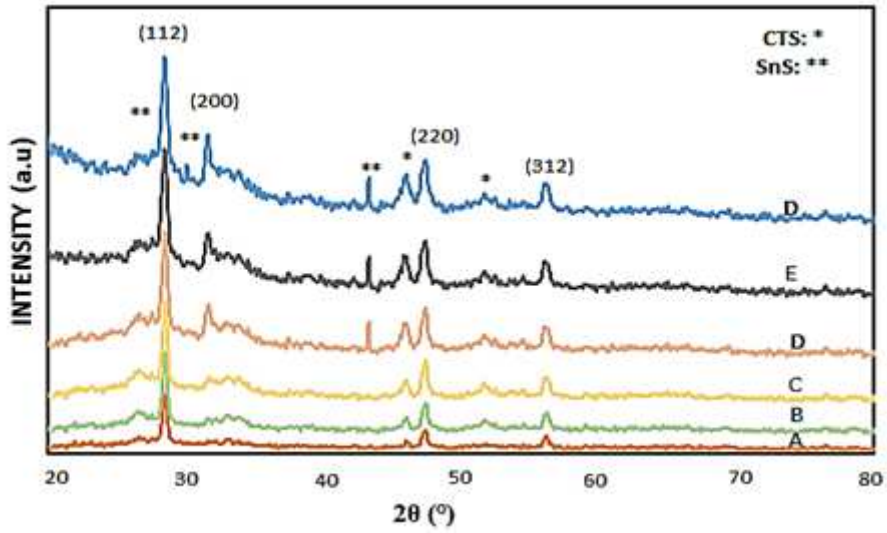

Figure 3

XRD Pattern of the CZTS layer heated at A) 300, B) 350, C) 400, D) 450, E) 500, and F) 550°C.

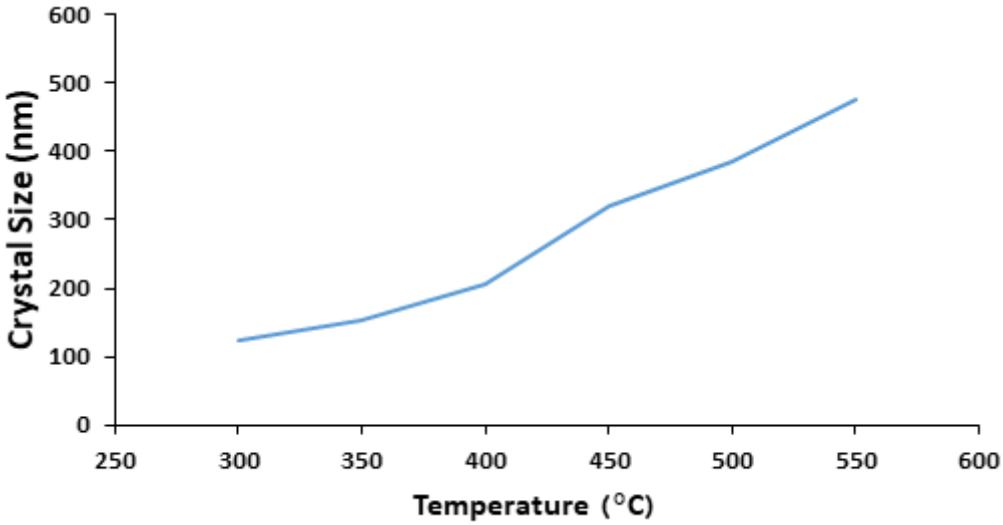

Figure 4

The average crystallite size of the samples.

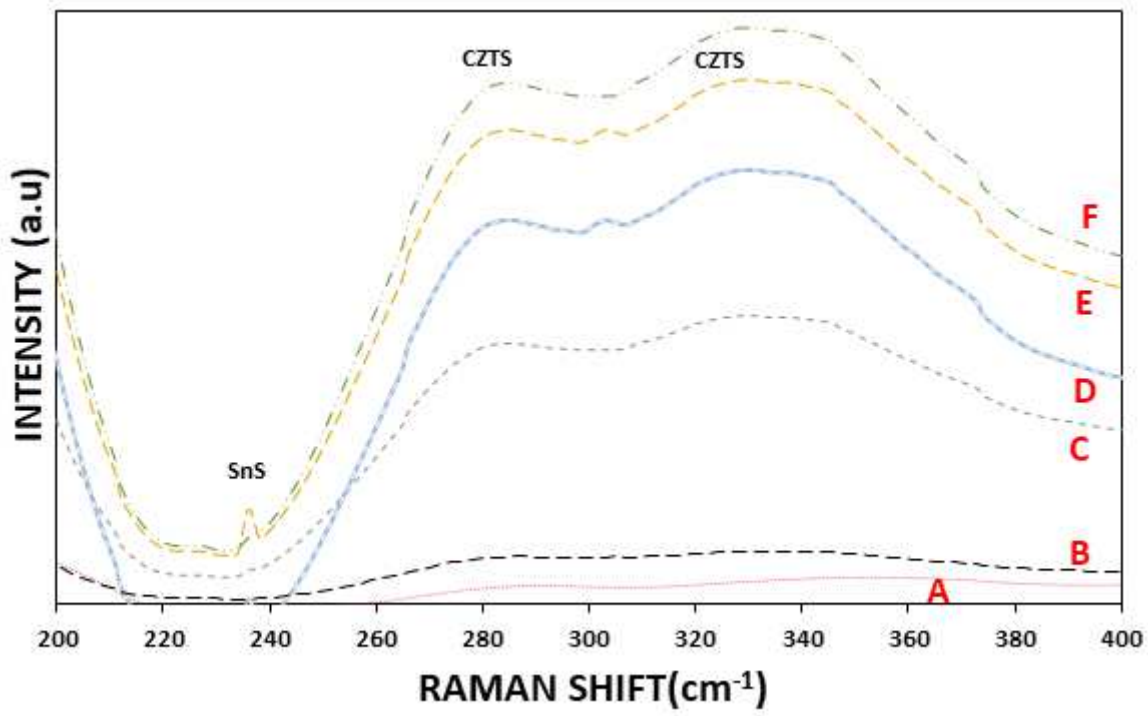

Figure 5

Raman spectra of CZTS films heated at A) 300, B) 350, C) 400, D) 450, E) 500, and F) 550 °C.

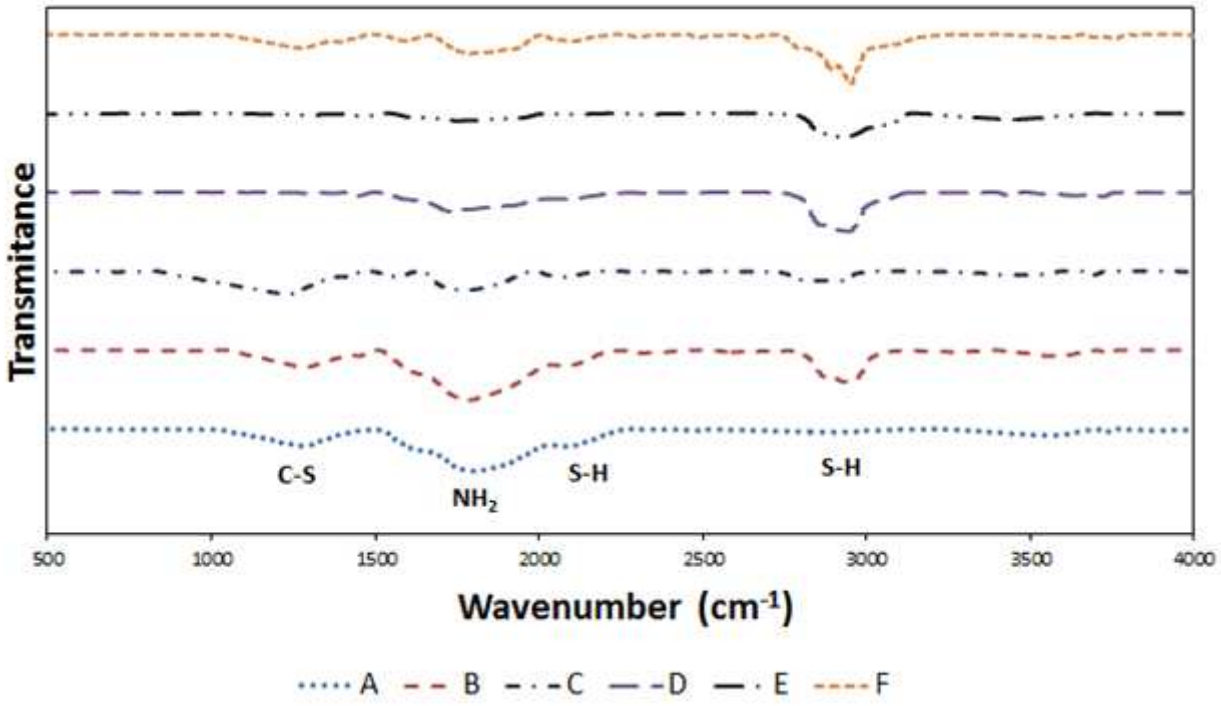

Figure 6

FTIR spectra of the CZTS samples heated at A) 300, B) 350, C) 400, D) 450, E) 500, and F) 550°C.

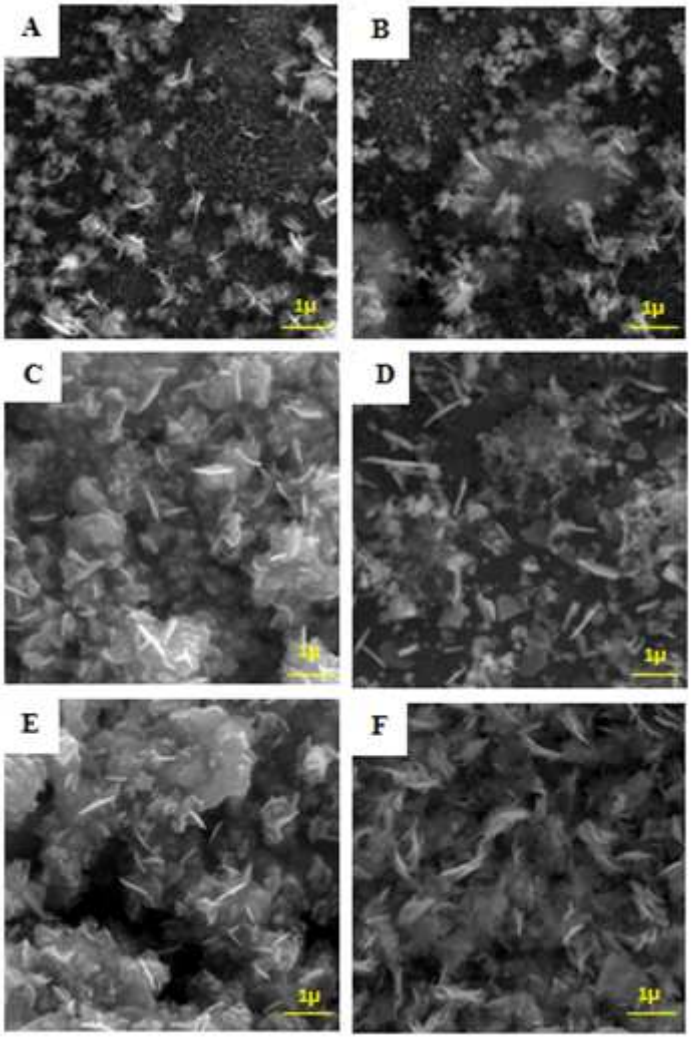

Figure 7

FESEM of CZTS layer prepared at (A) 300, (B) 350, (C) 400, (D) 450, (E) 500 and (F) 550°C.

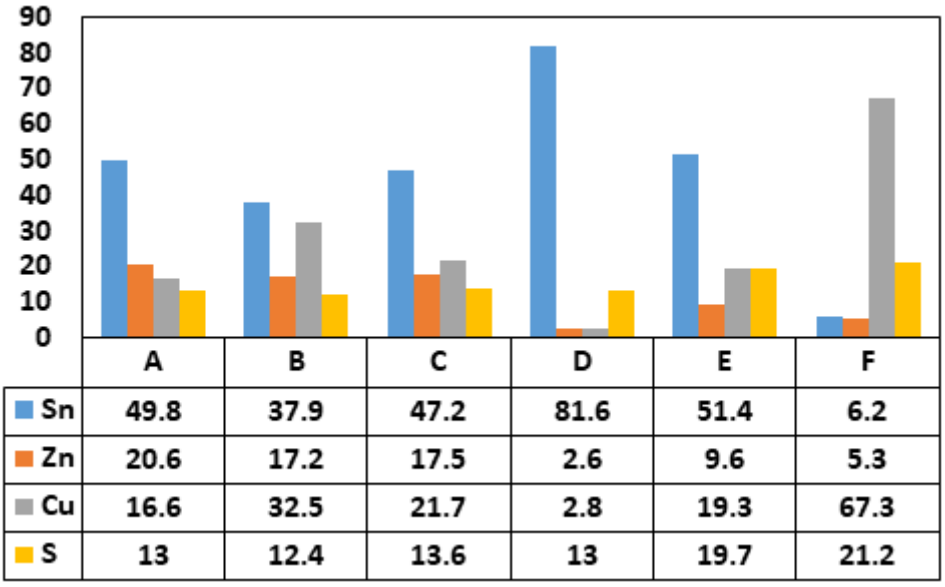

	A	B	C	D	E	F
Sn	49.8	37.9	47.2	81.6	51.4	6.2
Zn	20.6	17.2	17.5	2.6	9.6	5.3
Cu	16.6	32.5	21.7	2.8	19.3	67.3
S	13	12.4	13.6	13	19.7	21.2

Figure 8

Comparison of the EDS analysis of the CZTS layer synthesized at A) 300, B) 350, C) 400, D) 450, E) 500 and F) 550°C.

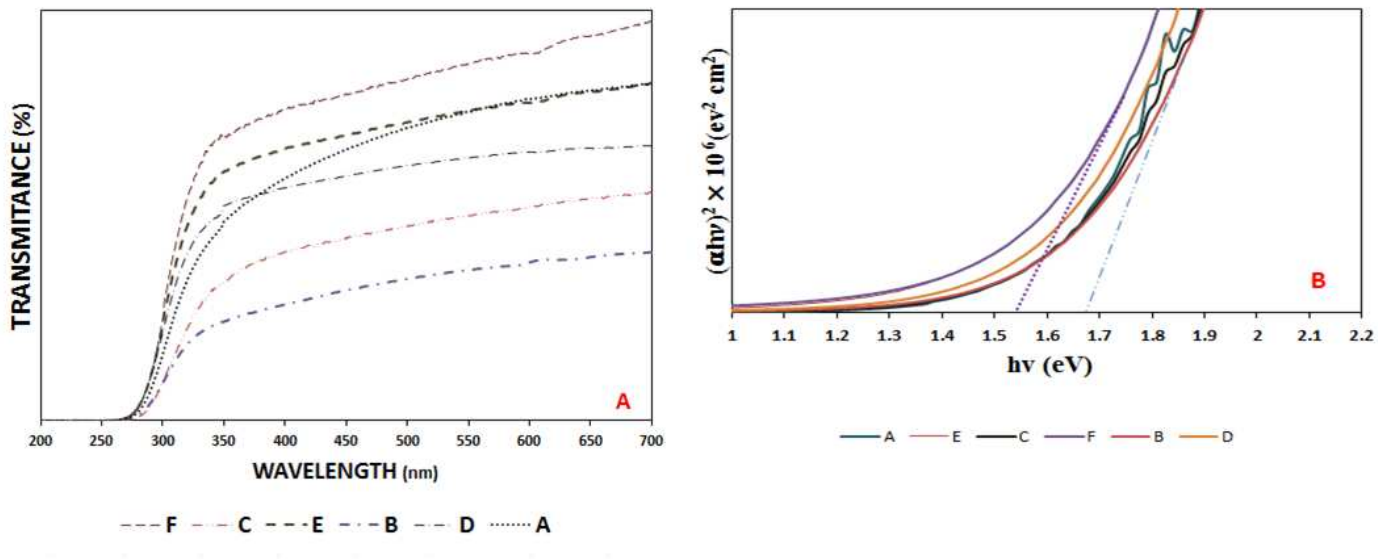

Figure 9

A) Transmittance spectra of the samples heated, B) The Tauc plot of the samples heated at A) 300, B) 350, C) 400, D) 450, E) 500 and F) 550°C.

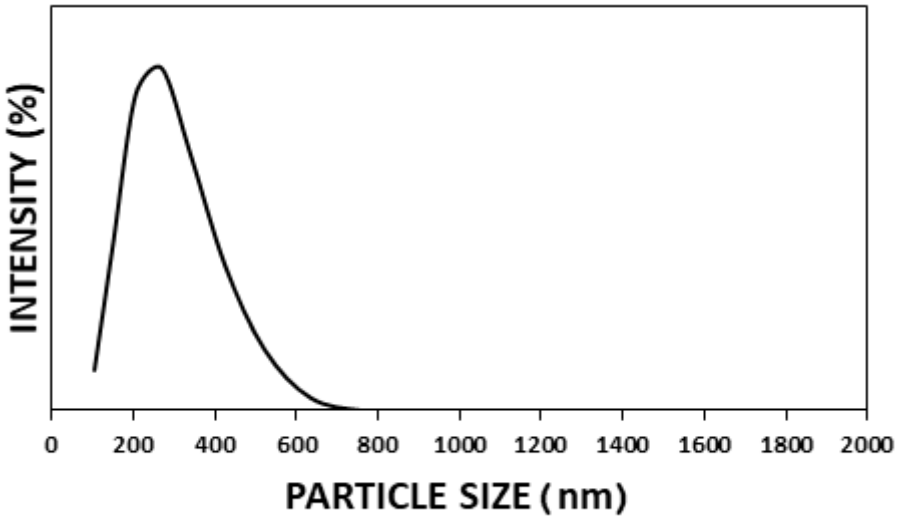

Figure 10

The particle size distribution curve of the synthesized powder at 500°C.